Available online at www.sciencedirect.com
ScienceDirect
Trans. Nonferrous Met. Soc. China 34(2024) 1380−1392
Transactions of Nonferrous Metals Society of China
www.tnmsc.cn

Intermetallic compounds in equilibrium with aluminum in Al−Ca−Cu ternary alloying system

T. K. AKOPYAN, T. A. SVIRIDOVA, N. A. BELOV, N. V. LETYAGIN, A. V. KOROTITSKIY

National University of Science and Technology MISiS, 4 Leninsky pr., Moscow 119049, Russia

Received 31 August 2022; accepted 21 March 2023

Abstract: The structure and properties of the new $(Al,Cu)_4Ca$, $Al_{27}Ca_3Cu_7$, and Al_8CaCu_4 intermetallic compounds in equilibrium with aluminum solid solution in the ternary Al−Ca−Cu alloying system were comprehensively analyzed. The $(Al,Cu)_4Ca$ intermetallic compound is treated as a line phase based on the Al_4Ca phase with Cu substituted by Al. The solubility of copper in the compound reaches 10 at.% (19 wt.%), which leads to marked changes in the crystal lattice structure, physical and mechanical properties of the compound. For instance, the density of the compound increases from 2.22 to 2.79 g/cm^3 and the microhardness from HV 180 to HV 250. The $Al_{27}Ca_3Cu_7$ phase is treated as a strict stoichiometric ternary compound with a primitive $BaHg_{11}$ type crystal structure of the *Pm*3*m* space group. The lattice parameter is accepted to be 8.514 Å corresponding to a density of 3.45 g/cm^3. The Al_8CaCu_4 phase is also a strict stoichiometric ternary compound with a tetragonal crystal lattice structure of the $Mn_{12}Th$ type. The phase has the highest microhardness (HV 505) and density (4.57 g/cm^3). The alloys pertaining to the binary (Al)+$(Al,Cu)_4Ca$ phase field and the quasi-binary (Al)+$Al_{27}Ca_3Cu_7$ section can be considered promising as the base for new natural aluminum matrix composites.

Key words: intermetallics; Al−Ca alloys; microstructure; crystal structure; physical properties; mechanical properties

1 Introduction

The Al−Cu−RE-based (RE represents rare earths) alloying systems have earned special attention in the design of new aluminum alloys [1−5]. Although the Al−Cu−RE system has been studied for the last fifteen years, the structure of the Al−Cu−RE phase diagram remains controversial. It was suggested that two quasi-binary sections Al−Al_8CeCu_4 and Al−Al_4CeCu exist in the Al-rich corner [6]. However, based on more recent studies [7−9] the Al_4CeCu phase is supposed to be Al_4Ce with Cu substituted by Al. Later, the Al_4RE ($(Al,Cu)_4RE$) type phase was treated as the $Al_{11}RE_3$ ($(Al,Cu)_{11}RE_3$) phase with the *Immm* space group in Al/heavy rare earth systems [10−12]. The Al_8CeCu_4 phase is treated as a strict ternary stoichiometric intermetallic compound with a $Mn_{12}Th$ type structure and the *I*4/*mmm* space group. Thus, the typical structure of the Al−Cu−RE-based alloys should consist of intermetallic compounds formed during alloy solidification via different eutectic transformations. It is well known that this type of structure is quite beneficial for additive manufacturing techniques [13−15]. However, despite the advantages of the Al−Cu−RE-based alloys such as good manufacturability and mechanical properties at room and elevated temperatures [1,3,7,15], the high cost of RE and to a less extent Cu, coupled with the relatively high density of both RE and Cu may hinder the widespread application of this group of alloys.

Alternative approach is transition to the systems based on the Al−Ca eutectic. Indeed, recent studies [16−19] revealed that Al−Ca-based alloys

Corresponding author: T. K. AKOPYAN, E-mail: nemiroffandtor@yandex.ru
DOI: 10.1016/S1003-6326(24)66478-2

have a good combination of mechanical properties and manufacturability for casting and metal forming. One should note that according to the data available, the crystallographic structure of the compounds in binary Al−Ca and ternary Al−Ca-based systems is very similar to that of the corresponding Al−RE-based systems. For instance, studies of the aluminum corner of the ternary Al−Ca−La system [19,20] revealed significant mutual solubility between the Al_4(Ca,La) and Al_{11}(La,Ca)$_3$ line phases forming from the corresponding Al_4Ca and $Al_{11}La_3$ binary compounds. The solubility of La in Al_4(Ca,La) is 3.7 at.%, which leads to a change in the lattice parameters and to a decrease in the microhardness by 16% (from HV 178 to HV 150). The solubility of Ca in Al_{11}(La,Ca)$_3$ is about 13.5 at.%, which means that about 67.5% of the lanthanum atoms are replaced by calcium in the compound. The observed change in the structure and composition of the compound leads to a marked decrease in its microhardness (from HV 404 to HV 330) and density (from 3.94 to 2.92 g/cm^3). One should note that the possibility of varying the physical and mechanical properties of intermetallic compounds by changing their chemical composition in the manner described above seems to be a promising approach to the modification of the final properties of the eutectic type alloys with a natural composite structure (the fraction of extra phases not less than 10 vol.%).

Study of the aluminum corner of the Al−Ca−Fe system [21] revealed that the ternary $Al_{10}CaFe_2$ compound is in equilibrium with aluminum by analogy with $Al_{10}CeFe_2$ [22] in the ternary Al−Ce−Fe system. Although the ternary Al−Ca−Cu system has not been previously studied, preliminary analysis of cast [23] and wrought [24] Al−Ca−Cu alloys demonstrated its prospects for the design of new aluminum alloys. Since the knowledge of phase equilibria is a fundamental issue for the design of alloys, the primary aim of this work is to describe the structure of the ternary system by identifying the compounds that are in equilibrium with aluminum. The comprehensive analysis made in this work revealed four intermetallic compounds that are in equilibrium with (Al) in the Al−Ca−Cu ternary system: the well-known strict stoichiometric binary compound Al_2Cu, the (Al,Cu)$_4$Ca line phase which is based on the Al_4Ca phase with Cu substituted by Al, and two previously undescribed strict stoichiometric ternary compounds: Al_8CaCu_4 and $Al_{27}Ca_3Cu_7$. One should note that the Al_8CaCu_4 phase has the same structural type ($Mn_{12}Th$) as the Al_8CeCu_4 phase, while the $Al_{27}Ca_3Cu_7$ phase is unique for the Al−Ca−Cu system. The data obtained can be further used for the complete description of the Al−Ca−Cu ternary system (for instance, using CALPHAD approach) [25−27].

2 Experimental

Several model alloys of the Al−Ca−Cu system (Table 1) were studied. The alloys were prepared from 99.99 wt.% aluminum in a resistance furnace (GRAFICARBO) with a graphite crucible. Aluminum was placed in the crucible, and after its melting, copper in the form of pure metal (99.9 wt.% Cu) and calcium in the form of binary Al−15%Ca master alloy were introduced into the melt. After melting of the main components, the melt was held for 5−10 min to obtain a homogeneous composition, and the metal was cast into a 10 mm × 20 mm × 180 mm graphite mold. The cooling rate in the mold was about 10 K/s. For achieving an equilibrium phase composition, some alloys were remelted and slowly solidified in the furnace chamber at a cooling rate of about 0.01 K/s.

Table 1 Chemical compositions of experimental alloys

No.	Alloy	Composition/wt.% (at.%)		
		Al	Ca	Cu
1	Al16Ca	Bal.	16.3(11.2)	−
2	Al8Ca1Cu	Bal.	7.8(5.2)	1.4(0.6)
3	Al7Ca2Cu	Bal.	6.8(4.6)	2.5(1.1)
4	Al6Ca3.5Cu	Bal.	5.7(3.8)	3.7(1.6)
5	Al6.75Cu2.25Ca	Bal.	2.2(1.5)	7.4(3.2)
6	Al14Cu10Ca	Bal.	9.5(7.0)	13.0(6.0)
7	Al14Cu12Ca	Bal.	11.0(8.1)	14.0(6.5)
8	Al26Cu8Ca	Bal.	7.5(5.8)	24.0(11.8)
9	Al27Cu4Ca	Bal.	3.5(2.7)	27.0(13.3)
10	Al32Cu2.5Ca	Bal.	2.1(1.7)	32.0(16.3)
11	Al22Cu2Ca	Bal.	2.3(1.7)	19.0(8.8)

The microstructure was examined by means of scanning electron microscopy (SEM, TESCAN VEGA 3) and electron microprobe analysis (EMPA, OXFORD AZtec). Polished samples were used for

the studies. Mechanical polishing was used, as well as electrolytic polishing at 12 V in an electrolyte with $C_2H_5OH/HClO_4$/glycerine volume ratio of 6:1:1.

X-ray diffraction (XRD) data were collected using Cu K_α or Co K_α radiation and treated with a software package [28]. The specimens for the X-ray diffraction study were polished specimens cut from part of the ingots or powder. The XRD data were used to determine the volume fractions and the lattice parameters of the phases. The relative error of the measurements was 10% for volume fraction and 0.15% for lattice parameter.

A dilatometric study was carried out at a heating rate of ~0.17 K/s on a quenching dilatometer DIL 805A/D (with the possibility of sample deformation by compression (TA Instruments, Germany)) with thermocouples (S-type) under vacuum (~0.013 Pa) for cylindrical samples with 6 mm in diameter and 12 mm in length.

The microhardness was determined on a DUROLINE MH−6 instrument (load of 0.05−0.10 kg and dwell time of 10 s).

In order to facilitate the preliminary analysis of the ternary system, a thermodynamic calculation was initially conducted using the Thermo-Calc software and the TTAL5 database [29].

3 Results and discussion

3.1 Preliminary theoretical and experimental analysis

At the beginning, ternary equilibrium in the aluminum corner of the Al−Ca−Cu system was calculated using the Thermo-Calc software and the TTAL5 database. Liquidus surfaces in the Al−Ca−Cu system for variable Ca and Cu contents were calculated for defining the area of primary crystallization of the aluminum solid solution (Al) (Fig. 1(a)). To verify the calculated data, some

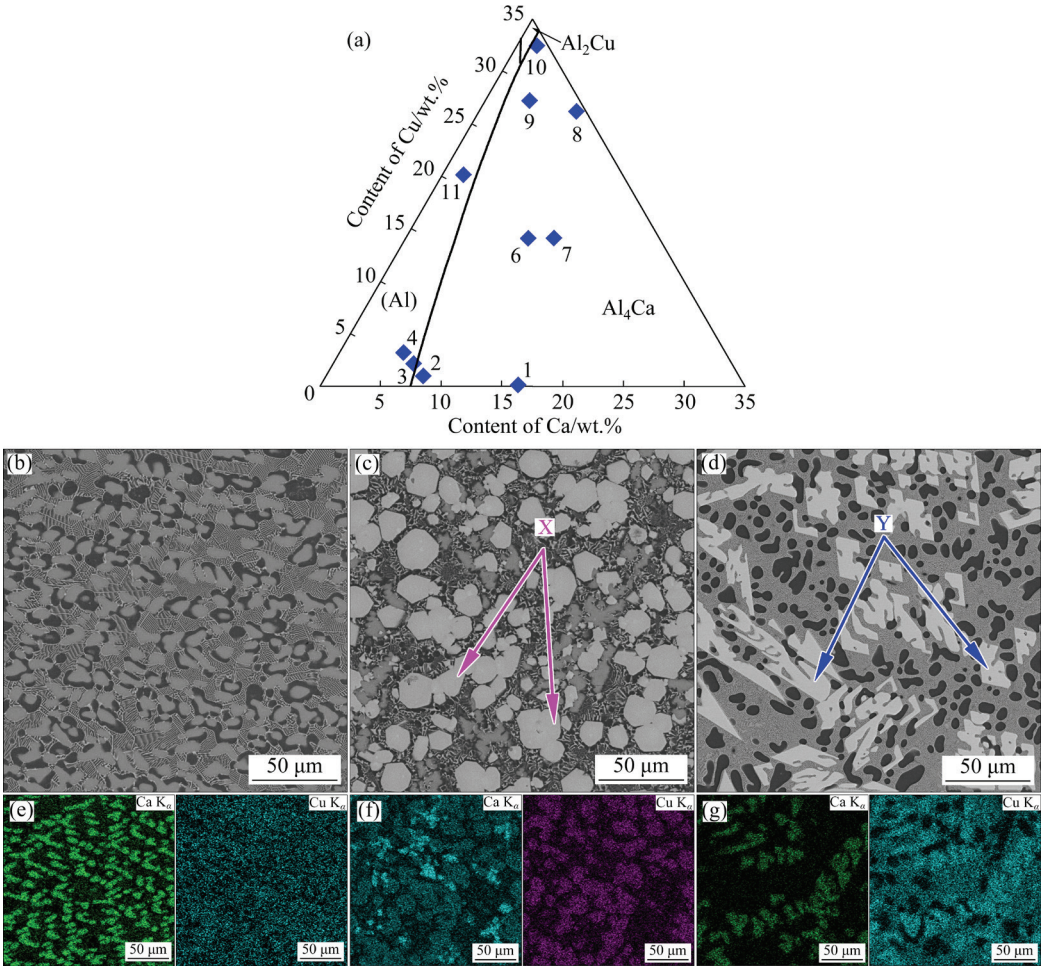

Fig. 1 Calculated polythermal projection of Al−Ca−Cu system (a) and microstructures of Al14Cu10Ca (b), Al26Cu8Ca (c) and Al36Cu2.5Ca (d) alloys in as-cast state (cooling rate ~10 K/s), and element mappings for alloys Al14Cu10Ca (e), Al26Cu8Ca (f) and Al32Cu2.5Ca (g)

alloys (marked on the diagram) were studied experimentally. It can be seen that the alloys are predominant in the hypereutectic area.

According to the calculated data, the aluminum solid solution (Al) can be in equilibrium with the two well-known Al_4Ca and Al_2Cu intermetallic compounds, and the main parameters of which are summarized in Table 2. However, a microstructural study of the experimental alloys revealed significant differences in the phase composition compared to the calculated data. Figure 1 shows the structure of the three alloys, where the Al14Cu10Ca (No. 6) and Al26Cu8Ca (No. 8) alloys pertain to the Al_4Ca phase primary crystallization field, and the third alloy, Al32Cu2.5Ca (No. 10), is at the boundary between the primary crystallization fields of the Al_2Cu and Al_4Ca phases. One can see that for the Al14Cu10Ca alloy (Fig. 1(b)), due to the intense calcium saturation (Fig. 1(e)), the primary crystals can be attributed to the Al_4Ca phase, and for the second (Fig. 1(c)) and third (Fig. 1(d)) alloys, a different type of primary crystals simultaneously saturated with calcium and copper (Figs. 1(f) and (g)) are observed. Thus, the results suggest that these primary crystals belong to new compounds since there are no data on copper- or calcium-containing phases. Detailed experimental studies of the structure and phase composition of some Al−Ca−Cu alloys were carried out in order to reveal their structure and properties. Some of the studies were carried out for slowly solidified alloys (melt cooling rate of ~0.01 K/s) which are expected to have a near-equilibrium phase composition. Each intermetallic compound will be separately analyzed below.

3.2 Al_4Ca compound

Al_4Ca compound is the predominant second phase in Al−Ca-based alloys and thus its properties mainly determine those of the alloys. The structure of the binary Al_4Ca compound formed in the base Al16Ca alloy was used as a reference for further studies. One can see from Table 3 that the content of the Al_4Ca phase in the alloy is about 60 vol.%, i.e., higher than that of the aluminum solid solution (Al). The data on the fractions of the compounds presented in Table 3 were obtained using experimental XRD studies and calculations based on simple stoichiometric balance corresponding to the alloy composition (see Eqs.(1)−(3)).

$$\begin{cases} C_{\mathrm{Al}_{(\mathrm{Al})}} Q_{(\mathrm{Al})} + C_{\mathrm{Al}_{\mathrm{X}}} Q_{\mathrm{X}} + C_{\mathrm{Al}_{\mathrm{Y}}} Q_{\mathrm{Y}} = C_{\mathrm{AAl}} \\ C_{\mathrm{Ca}_{(\mathrm{Al})}} Q_{(\mathrm{Al})} + C_{\mathrm{Ca}_{\mathrm{X}}} Q_{\mathrm{X}} + C_{\mathrm{Ca}_{\mathrm{Y}}} Q_{\mathrm{Y}} = C_{\mathrm{ACa}} \\ C_{\mathrm{Cu}_{(\mathrm{Al})}} Q_{(\mathrm{Al})} + C_{\mathrm{Cu}_{\mathrm{X}}} Q_{\mathrm{X}} + C_{\mathrm{Cu}_{\mathrm{Y}}} Q_{\mathrm{Y}} = C_{\mathrm{ACu}} \end{cases} \quad (1)$$

Table 2 Parameters of phases [31] in Al-rich corner of Al−Ca−Cu system

Phase	Composition		Crystal lattice	Density/(g·cm^{-3})	Hardness (HV)
	wt.%	at.%			
Al_4Ca	27Ca	20Ca	Tetragonal, *I*4/*mmm*; Pearson symbol: tI10; *a*=4.36 Å; *c*=11.09 Å	2.35	200
Al_2Cu	55Cu	33Cu	Orthorhombic, *Pnma*; Pearson symbol: oP16; *a*=6.61 Å, *b*=7.37 Å, *c*=4.81 Å	3.95	700−770

Table 3 Chemical composition, calculated and experimentally determined mass fraction (Q_m), volume fraction (Q_v) and microhardness (HV) for $(Al,Cu)_4Ca$ compound detected in alloys obtained at specific cooling rate (v_s) upon solidification

Alloy	v_s/(K·s^{-1})	Phase	Chemical composition (EMPA)/at.% (wt.%)			Q_m (Q_v) (Calc. data)/%	Q_v(XRD data)/%	Hardness (HV)
			Al	Ca	Cu			
Al16Ca	~10	Al_4Ca	Bal.	20±0.2(28±0.3)	−	53(58)	60±1.5	180
Al8Ca1Cu	~10	$(Al,Cu)_4Ca$	Bal.	20±0.2(27±0.3)	2.1±0.2(5±0.3)	30(34)		
Al7Ca2Cu	~10	$(Al,Cu)_4Ca$	Bal.	19.3±0.2(26±0.3)	3.5±0.2(7±0.3)	26(28)		
Al6Ca3.5Cu	~0.01	$(Al,Cu)_4Ca$	Bal.	19.0±0.2(24±0.3)	6.5±0.2(13±0.3)	21(23)	28	
Al14Cu10Ca	~10	$(Al,Cu)_4Ca$	Bal.	20.0±0.2(25±0.3)	8.0±0.2(16±0.3)	31(33)	28	270
Al26Cu8Ca	~10	$(Al,Cu)_4Ca$	Bal.	20.0±0.2(25±0.3)	10.0±0.2(19±0.3)	6.5(7.7)	10	

$$\Delta = \begin{bmatrix} C_{Al_{(Al)}} & C_{Al_X} & C_{Al_Y} \\ C_{Ca_{(Al)}} & C_{Ca_X} & C_{Ca_Y} \\ C_{Cu_{(Al)}} & C_{Cu_X} & C_{Cu_Y} \end{bmatrix} \quad (2)$$

$$\Delta^{-1} \begin{bmatrix} C_{AAl} \\ C_{ACa} \\ C_{ACu} \end{bmatrix} = \begin{bmatrix} Q_{(Al)} \\ Q_X \\ Q_Y \end{bmatrix} \quad (3)$$

where C_{AAl}, C_{ACa} and C_{ACu} are the concentrations (wt.%) of Al, Ca and Cu in the alloy, respectively, $C_{Al_{(Al),X,Y}}$, $C_{Ca_{(Al),X,Y}}$, $C_{Cu_{(Al),X,Y}}$, are the concentrations (wt.%) of Al, Ca and Cu in (Al), and X and Y phases with the mass fractions $Q_{(Al)}$, Q_X and Q_Y, respectively. Then, with the known density of the compounds, the mass fraction was recalculated to volume fraction. The density of the compounds was calculated using the XRD data on the crystal structure.

According to the available information on the structure of the binary Al−Ca phase diagram [30], the eutectic point in the aluminum corner corresponds to ~7.6 wt.% Ca. As can be seen from Fig. 2(a), the structure of the Al16Ca alloy is strongly hypereutectic and contains coarse Al_4Ca phase primary crystals having a plate-like feather structure. EMPA analysis confirmed that the observed crystals correspond perfectly well to the known stoichiometric composition (Table 2) and have a microhardness of about HV 180 which is somewhat lower than the previously reported value [30]. Addition of 1 and 2 wt.% Cu in the Al8Ca and Al7Ca near eutectic alloys (Figs. 2(b−d)), respectively, still leads to the formation of a hypereutectic structure with a typical acicular shape of primary crystals. Due to the relatively fine structure of the primary crystals in the Al7Ca2Cu alloy (Fig. 2(c)), it was also obtained after slow solidification leading to the formation of much coarser primary crystals that can be used for composition measurement. EMPA analysis of the primary crystals in both alloys revealed that the Ca concentration is still in a good agreement with the stoichiometric one of 20 at.% while additional dissolution of copper in the compound was also observed (Table 3). It was assumed that the observed compound is the $(Al,Cu)_4Ca$ phase with Cu substituted by Al. Further XRD analysis confirmed this assumption (Fig. 3). The observed solubility increases with increasing copper content in the alloy. Indeed, for the next alloy in the series, i.e., Al6Ca3.5Cu, the solubility of copper reaches a significant 6.5 at.% (13 wt.%). One should note that this alloy has a fine eutectic structure (Fig. 2(e)) even after slow solidification (Fig. 2(f)), and the fraction of the $(Al,Cu)_4Ca$ intermetallic compound reaches 28 vol.% (Table 3). It is worth nothing that for another aluminum eutectic system Al−Si which is currently used in the design of alloys most widely used for the SLM technique, the maximum fraction of eutectic crystals is about 12 vol.% while for the

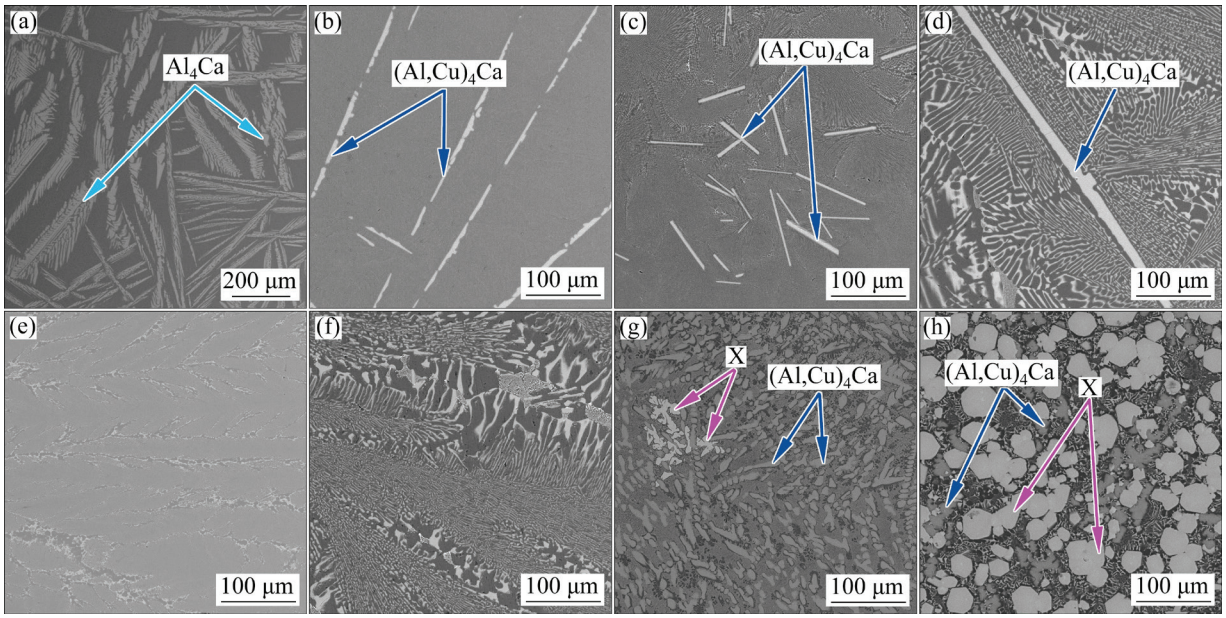

Fig. 2 SEM images of alloys at cooling rates of 10 K/s (a, b, c, e, g, h) and 0.01 K/s (d, f): (a) Al16Ca; (b) Al8Ca1Cu; (c, d) Al7Ca2Cu; (e, f) Al6Ca3.5Cu; (g) Al14Cu10Ca; (h) Al26Cu8Ca

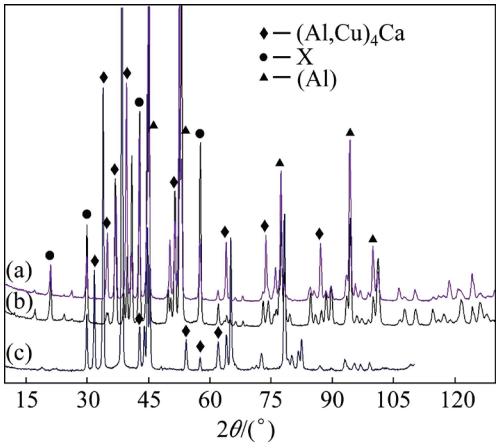

Fig. 3 XRD patterns for Al14Cu10Ca (Co K_α radiation) (a), Al26Cu8Ca (Co K_α radiation) (b) and Al6Ca3.5Cu (Cu K_α radiation) (c) alloys

Al−Ce−Cu system it is even lower. Thus, alloys based on the new system can be considered as natural composites which have a superior fraction of the extra phases among other aluminum-based systems, thus providing for high strengthening by the Orowan mechanism [31,32].

The Al8Ca1Cu, Al7Ca2Cu and Al6Ca3.5Cu alloys discussed above are located near the boundary between the binary and ternary phase fields (Al) + $(Al,Cu)_4Ca$/(Al) + $(Al,Cu)_4Ca$ + X(AlCaCu) and contain an insignificant amount of the third new X(AlCaCu) phase (discussed below). The studies were continued for alloys with a dominate content of copper located deep in the ternary (Al) + $(Al,Cu)_4Ca$ + X(AlCaCu) phase field. Figure 2(g) shows the strongly hypereutectic structure of the Al14Cu10Ca alloy. The observed two types of primary crystals contain the X(AlCaCu) and $(Al,Cu)_4Ca$ phases with the amount of the latter being the highest. It is worth noting that the morphology of the crystals turned too compact compared to the above-described acicular structure. The microstructural modification of the $(Al,Cu)_4Ca$ compound can be accounted for by the effect of changes in the crystal structure, resulting in an evolution of its chemical composition. EMPA studies revealed an additional increase in the copper solubility to 8 at.% (16 wt.%). Microhardness tests for $(Al,Cu)_4Ca$ primary crystals revealed the value of HV 270, much higher than HV 180 for the binary Al_4Ca compound (Table 3). The increase in the microhardness can be attributed to solid solution hardening. It is interesting to note that a substitution of about 20% of Ca atoms by La in the $Al_4(Ca,La)$ phase leads to a noticeable decrease in the microhardness of the compound by ~16% (from HV 178 to HV 150) [20].

A substantial increase in the copper content in the Al26Cu8Ca alloy (Fig. 2(h)) led to the formation of a large number of X(AlCaCu) phase primary crystals (bright in appearance and faceted). However, some $(Al,Cu)_4Ca$ primary crystals can still be observed, and their EMPA analysis revealed a further increase in the copper solubility to 10 at.% (19 wt.%). Subsequent variation of the alloy compositions did not reveal significant differences in the composition of the compound as compared to the above-described ones. The latter fact suggests that the experimental data on copper solubility in the $(Al,Cu)_4Ca$ intermetallic phase are comprehensive.

The crystal structure of the $(Al,Cu)_4Ca$ phase depending on its chemical composition was studied in detail using XRD. The results are presented in Table 4. The $(Al,Cu)_4Ca$ phase has a tetragonal D1.3 type structure. One can see that an increase in the copper solubility to 10 at.% leads to a marked decrease in the *a* parameter by about 3% and an increase in the *c* parameter by about 1%. The observed change in the lattice parameters reduces the atomic volume by about 10%. The decrease in the atomic volume coupled with the incorporation of heavy copper atoms leads to a gradual increase in the density of the compound. Indeed, the density of the base binary Al_4Ca compound was assessed to be

Table 4 Effect of copper solubility in $(Al,Cu)_4Ca$ phase on its crystal structure and density

Solubility of Cu/at.%	Lattice parameter (XRD data)/Å		Atomic volume/ 10^{-2} nm^3	Relative change in atomic volume/%	Density/ (g·cm^{-3})	Relative increase in density/%
	a	*c*				
0	4.372	11.282	2.156	0	2.22	0
6.5	4.228	11.356	2.030	−5.9	2.56	15.2
8	4.220	11.375	2.026	−6.1	2.61	17.5
10	4.212	11.392	1.934	−10.3	2.79	26.0

2.22 g/cm^3. Dissolution of 10 at.% Cu increases the compound density to 2.79 g/cm^3 which is somewhat higher than that of pure aluminum and 26% higher than that of the base binary compound.

3.3 $Al_{27}Ca_3Cu_7$ compound

Some of the alloys discussed above pertain to the ternary (Al) + $(Al,Cu)_4Ca$ + X(AlCaCu) phase field with a new previously undescribed ternary X(AlCaCu) compound. SEM (Fig. 4) and XRD (Fig. 5) studies were carried out to reveal its structure. As is shown for the Al26Cu8Ca alloy (Fig. 2(h)), its structure contains a large number of compact bright faceted crystals. Similar primary crystals are observed in the Al22Cu2Ca alloy (Fig. 4(a)). According to EMPA data, the crystals in both alloys have perfectly the same composition (Table 5). XRD revealed that these crystals have a primitive $BaHg_{11}$ type crystal structure with the

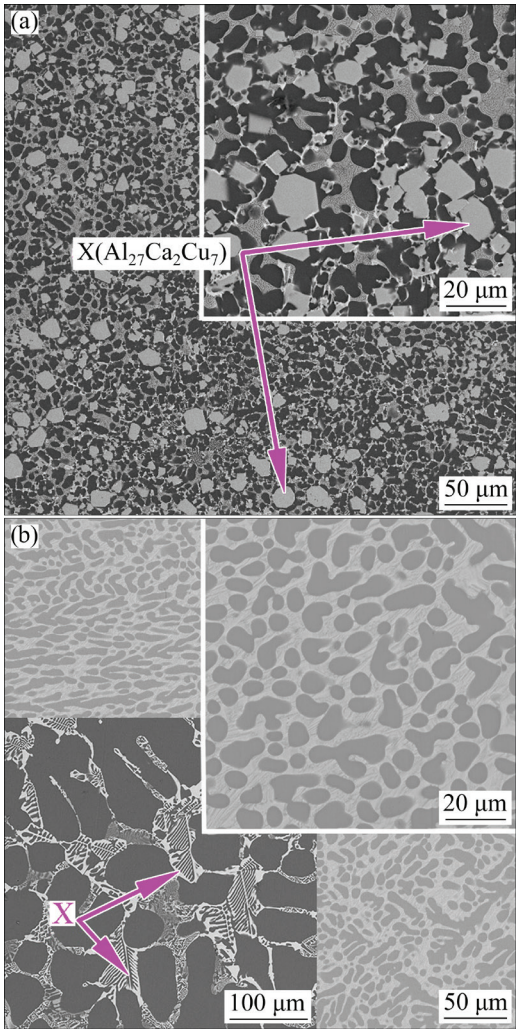

Fig. 4 SEM images of as-cast alloys at cooling rates of 10 K/s (background and top right) and 0.01 K/s (bottom left): (a) Al22Cu2Ca; (b) Al6.75Cu2.25Ca

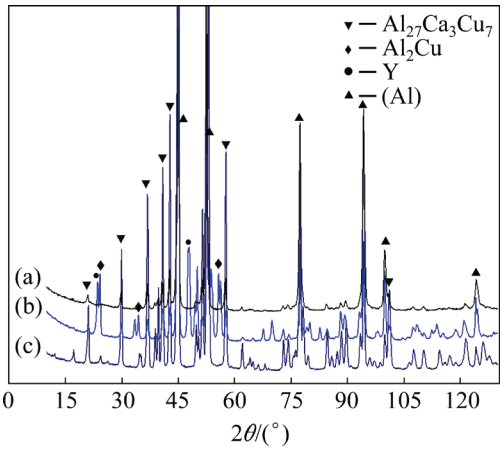

Fig. 5 XRD patterns for Al6.75Cu2.25Ca (Co K_α radiation) (a), Al22Cu2Ca (Co K_α radiation) (b) and Al26Cu8Ca (Co K_α radiation) (c) alloys

*Pm*3*m* space group (Pearson symbol tI10/1). Based on the SEM and XRD data, this intermetallic phase was treated as strict stoichiometric ternary compound having the formula $Al_{27}Ca_3Cu_7$. Based on the XRD data (Table 5), the lattice parameter can be evaluated as 8.514 Å corresponding to a compound density of 3.45 g/cm^3. The microhardness is HV 420, which is much higher than that of $(Al,Cu)_4Ca$ and also higher than that of the $Al_{11}RE_3$ type crystals for which it is HV 400. The described crystallographic structure of the phase is visualized in Fig. 6.

Figure 4(b) shows the structure of the new promising alloy consisting of fine eutectic. This alloy can also be considered a natural composite since, according to XRD, it contains about 16 vol.% intermetallic compounds ($Al_{27}Ca_3Cu_7$ + $(Al,Cu)_4Ca$) with the largest fraction of $Al_{27}Ca_3Cu_7$ (~13.5 vol.%, see Table 5). EMPA analysis of these crystals for slowly solidified alloy (Fig. 4(b)) revealed the same chemical composition (Table 5) as that of the primary crystals. Thus, the (Al) + $Al_{27}Ca_3Cu_7$ quasi-binary section can also be considered promising for the design of new aluminum-matrix alloys.

3.4 Al_8CaCu_4 compound

One more new strict stoichiometric ternary compound Y(AlCaCu) was found to be in equilibrium with aluminum in alloys with a predominant content of copper. In order to obtain a high fraction of this phase, the structure of the Al−(2.5−5)wt.%Ca−Cu alloys with a copper content close to the eutectic point in the binary

Table 5 Chemical composition, volume fraction (Q_v), lattice parameter, microhardness (HV) and calculated density of $Al_{27}Ca_3Cu_7$ phase detected in alloys obtained at specific cooling rate (v_s) upon solidification

Alloy	v_s/(K·s^{-1})	Chemical composition (EMPA)/at.% (wt.%)			Q_v (XRD data)/%	Lattice parameter a (XRD data)/Å	Hardness (HV)	Density/(g·cm^{-3})
		Al	Ca	Cu				
Al22Cu2Ca	10	Bal.	8.0(9.2)	21.0(38.1)	15	8.512		
Al26Cu8Ca	10	Bal.	8.0(9.2)	21.0(38.1)	56	8.516	420	3.45
Al6.75Cu2.25Ca	0.01	Bal.	8.0(9.2)	21.0(38.1)	13.5	8.514		

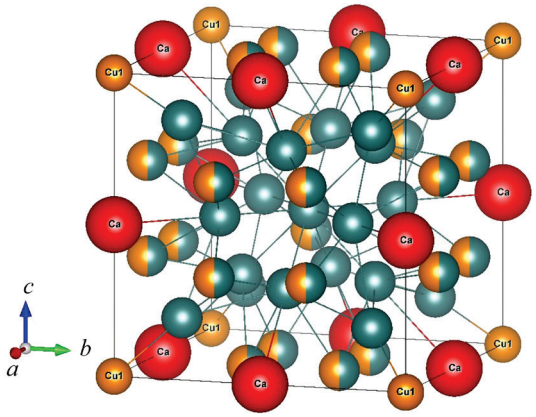

Fig. 6 Visualization of $Al_{27}Ca_3Cu_7$ phase crystal lattice

Al−Cu system was studied. Analysis of the alloys microstructure revealed the presence of a high amount of bright primary crystals with a faceted structure (Fig. 7). EMPA analysis showed the similar composition of those crystals (Table 6). The structure of the Al27Cu4Ca alloy also contains a minor fraction of gray primary crystals which, however, correspond to the $Al_{27}Ca_3Cu_7$ phase (Fig. 7(b)). XRD analysis (Fig. 8) revealed that the new crystals possess a tetragonal crystal lattice structure (Pearson symbol tI26/1) of the $Mn_{12}Th$ type same as for the well-known Al_8CeCu_4 phase of the ternary Al−Ce−Cu system. The new phase was treated as Al_8CaCu_4. The crystallographic structure of the phase is illustrated in Fig. 9. The microhardness (HV 505) and density (4.57 g/cm^3) of the Al_8CaCu_4 phase are the highest among the other Ca-containing phases in the system. However, alloys based on this compound seem to be of less interest due to the high content of heavy and expensive copper.

3.5 Phase fields distribution

As noted above, some alloys of the system, especially those in the binary (Al) + $(Al,Cu)_4Ca$ phase field and the quasi-binary (Al) + $Al_{27}Ca_3Cu_7$ section, are promising as the base of new natural aluminum matrix composites. Indeed, their fine as-cast

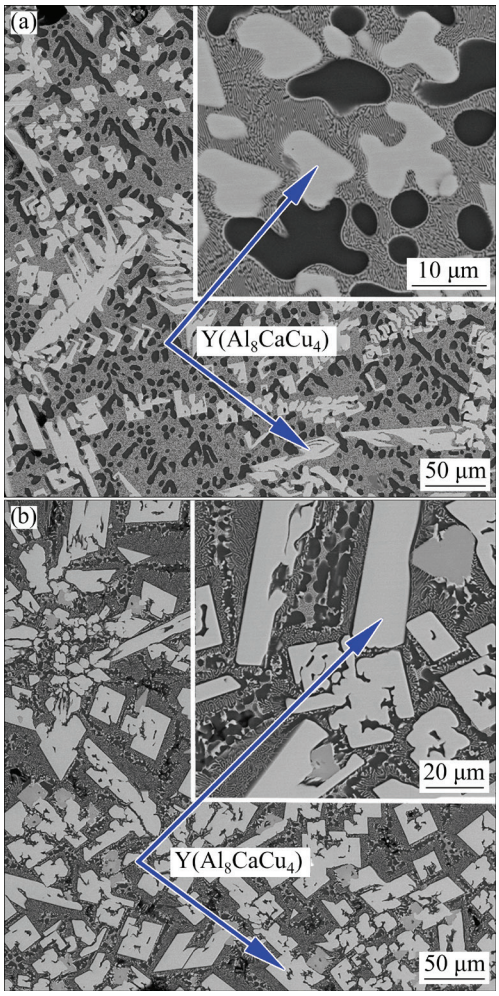

Fig. 7 SEM images of as-cast alloys at cooling rate of 10 K/s: (a) Al32Cu2.5Ca; (b) Al27Cu4Ca

structure coupled with a large fraction of the eutectic phases provides for the great potential of these alloys for the SLM technique. However, the design of new alloys requires information about the distribution of phase fields as a function of temperature and chemical composition. Although the construction of the liquidus projection in the Al−Ca−Cu ternary system requires further experimental studies, the distribution of phase fields in the solid state can be hypothesized based on the results of this work (Fig. 10). As can be seen from

Table 6 Chemical composition, volume fraction (Q_v), lattice parameter, microhardness (HV) and calculated density of Al_8CaCu_4 phase detected in alloys obtained at specific cooling rate (v_s) upon solidification

Alloy	v_s/(K·s^{-1})	Chemical composition (EMPA)/at.% (wt.%)			Q_v(XRD data)/%	Lattice parameter (XRD data)/Å		Hardness (HV)	Density/(g·cm^{-3})
		Al	Ca	Cu		*a*	*c*		
Al36Cu2.5Ca	10	Bal.	7.5(7.6)	33(53.1)	27	8.800	5.140		
Al27Cu4Ca	10	Bal.	7.5	33	51	8.803	5.141	505	4.57

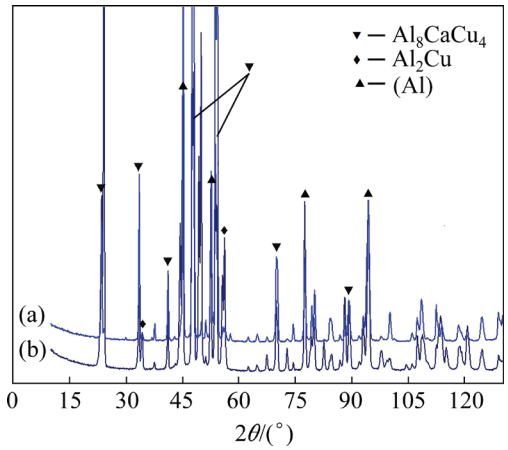

Fig. 8 XRD patterns for Al27Cu4Ca (Co K_α radiation) (a) and Al32Cu2.5Ca (Co K_α radiation) (b) alloys

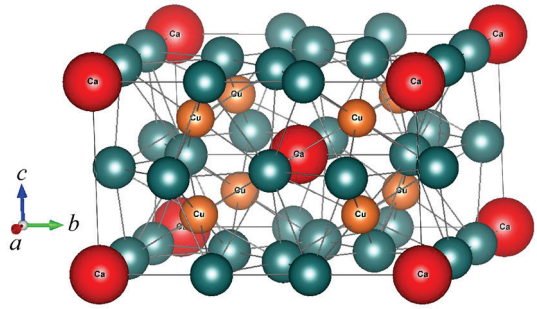

Fig. 9 Visualization of Al_8CaCu_4 phase crystal lattice

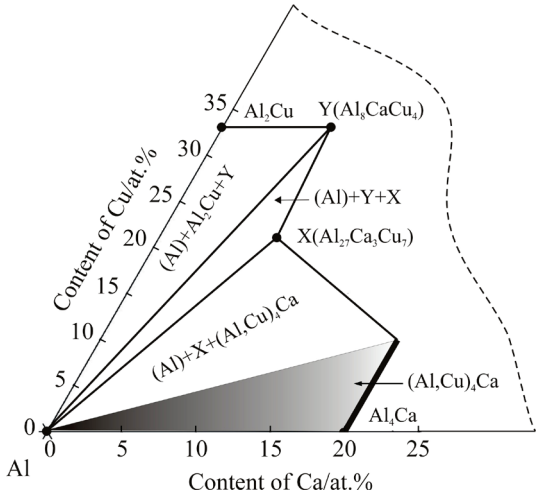

Fig. 10 Proposed phase field distribution in solid state at room temperature

Fig. 10, three ternary phase fields can be identified: (Al) + Al_2Cu + Al_8CaCu_4, (Al) + Al_8CaCu_4 + $Al_{27}Ca_3Cu_7$ and (Al) + $(Al,Cu)_4Ca$ + $Al_{27}Ca_3Cu_7$. Due to the noticeable solubility of copper in the $(Al,Cu)_4Ca$ phase, one can also observe the presence of the wide binary (Al) + $(Al,Cu)_4Ca$ phase field. Furthermore, two quasi-binary sections (Al) + Al_8CaCu_4 and (Al) + $Al_{27}Ca_3Cu_7$ should be noted. It can be seen that the experimental diagram revealed a much more complex structure compared to those suggested by the calculations. Further studies should be focused on the clarification and construction of the liquidus projection and phase field distribution in the system in the solid state at elevated temperatures (close to solidus) using both experimental data and the CALPHAD approach.

3.6 Coefficient of thermal expansion

Due to the high fraction of extra phases, the coefficient of thermal expansion (CTE) is among the main specific properties of natural composites in contrast to conventional alloys. Moreover, CTE largely determines the generation of thermal stresses and thus the manufacturability of the materials for casting or SLM techniques. Some alloys with a high fraction of the extra phase were subjected to dilatometric studies in order to assess the CTE of the new compounds. The chosen alloys and the XRD data on their phase fractions are presented in Table 7. It was assumed that the contributions of the phases constituting the alloys can be taken into account additively in accordance with their fraction in the alloy. One should also note that due to the very limited solubility of Ca in the aluminum solid solution [30], the fraction of the Ca-containing phases can be accepted to be constant over the entire temperature range covered by the analysis. It is convenient to start the analysis from two-phase alloys containing an intermetallic phase along with aluminum. Knowing the fraction of the phases, as well as the CTE temperature dependences for the alloy and for one of the known

phase components (e.g. for aluminum), one can assess the CTE temperature dependence for the other phase. To confirm the assumption about the additive contribution of the phase components to the overall CTE of the alloy, the binary Al16Ca alloy containing about 62 vol.% Al_4Ca phase was used for the analysis of the CTE of the compound and the obtained data were compared with the reference data.

Table 7 XRD-determined fractions of phases in alloys used for CTE measurement

Alloy	Content/vol.%			
	$(Al,Cu)_4Ca$	$Al_{27}Cu_7Ca_3$	Al_8CaCu_4	Al_4Ca
Al27Cu4Ca	–	–	51	–
Al26Cu8Ca	10	56	–	–
Al14Cu12Ca	40	17	–	–
Al14Cu10Ca	28	21	–	–
Al16Ca	–	–	–	62

The initially obtained CTE curves for the alloys are shown in Fig. 11(a). One can note that all the CTE values are somewhat lower than those for pure aluminum. However, although the total fractions of the extra phases in all the studied alloys are comparable, the Al16Ca alloy has the lowest CTE. Moreover, starting from about 250 °C, the CTE curve shows a gradual decrease in the entire remaining temperature range up to 500 °C. Based on the above assumption, a CTE curve was extracted for the Al_4Ca compound (Fig. 11(b)). One can see that below 250 °C the CTE varies slightly and is about 16×10^{-6} K^{-1}. Starting from this point the CTE shows a gradual decline, reaching ~11×10^{-6} K^{-1} at 500 °C. It was reported in Refs. [33−35] that the CTE of Al_4Ca is 14×10^{-6} K^{-1} (average for a range of 20−300 °C), which is quite close to the assessment made in this work. Dilatometric study of the Al27Cu4Ca alloy containing about 50 vol.% Al_8CaCu_4 phase allowed drawing its CTE curve (Fig. 11(b)). One can see that the CTE varies slightly with temperature and can be accepted to be 18×10^{-6} K^{-1} at 200−500 °C. Study of the Al26Cu8Ca alloy allowed constructing the CTE curve of the $Al_{27}Cu_7Ca_3$ compound. It is somewhat higher than that of Al_8CaCu_4 and can be accepted to be $(20-21)\times10^{-6}$ K^{-1} at 200−500 °C. The CTE for the $(Al,Cu)_4Ca$ compound was also assessed using the data obtained for the Al14Cu10Ca alloy. One can see that Cu dissolution in Al_4Ca leads to a noticeable increase in its CTE. Indeed, the CTE slightly varies with temperature and is about 20×10^{-6} K^{-1} compared to $(11-16)\times10^{-6}$ K^{-1} for the base binary Al_4Ca compound. For additional confirmation of the correctness of the CTE data for the compounds, the CTE of the Al14Cu10Ca alloy (Table 7) was calculated based on this data and compared with the experimental CTE curve (Fig. 11(a)). One can see that the calculated curve describes the experimental curve adequately well thus confirming the above data on the CTE of the new compounds.

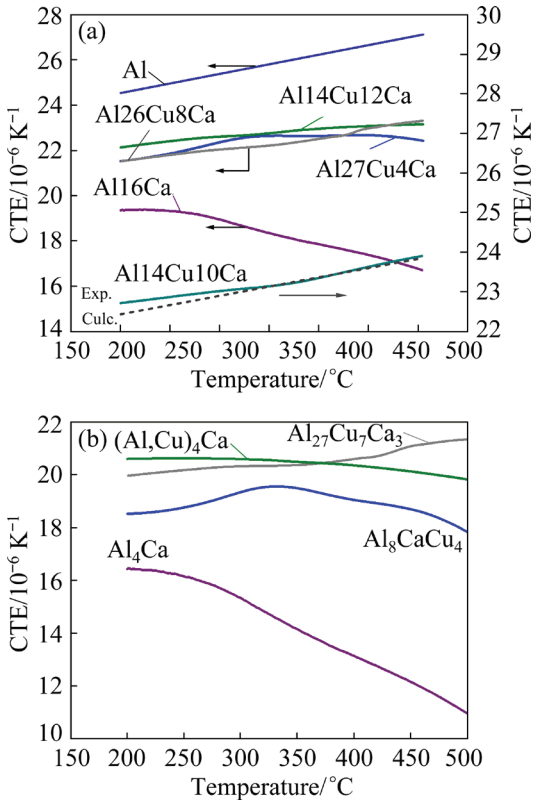

Fig. 11 Coefficient of thermal expansion as function of temperature for Al27Cu4Ca, Al26Cu8Ca, Al14Cu12Ca and Al16Ca alloys and experimental and calculated (dashed line) curves for Al14Cu10Ca alloy (a), and for Al_4Ca, $(Al,Cu)_4Ca$, $Al_{27}Cu_7Ca_3$ and Al_8CaCu_4 compounds (b)

4 Conclusions

(1) Study of the ternary Al−Ca−Cu system revealed that aluminum solid solution (Al) can be in equilibrium with four intermetallic compounds: $(Al,Cu)_4Ca$, $Al_{27}Ca_3Cu_7$, Al_8CaCu_4 and Al_2Cu, of which the former three are described for the first

time. In the solid state the identified phases can be distributed in the three (Al) + Al_2Cu + Al_8CaCu_4, (Al) + Al_8CaCu_4 + $Al_{27}Ca_3Cu_7$ and (Al) + $(Al,Cu)_4Ca$ + $Al_{27}Ca_3Cu_7$ ternary phase fields and the wide (Al) + $(Al,Cu)_4Ca$ binary phase field.

(2) $(Al,Cu)_4Ca$ intermetallic compound was treated as a line phase based on the Al_4Ca phase with Cu substituted by Al. It is shown that the solubility of copper in the compound reaches 10 at.% (19 wt.%), which leads to marked changes in the structure, physical and mechanical properties of the compound. For example, the atomic volume decreases by about 10% (from 2.156×10^{-2} to 1.934×10^{-2} nm^3), which couples with the incorporation of heavy copper atoms and increases the density of the compound from 2.22 g/cm^3 for the binary Al_4Ca phase to 2.79 g/cm^3 for the $(Al,Cu)_4Ca$ solid solution. The material also exhibits a substantial increase in the microhardness (from HV 180 to HV 250) and the coefficient of thermal expansion (from $(11-16)\times10^{-6}$ to 20×10^{-6} K^{-1} at 200−500 °C).

(3) The $Al_{27}Ca_3Cu_7$ phase was treated as a strict stoichiometric ternary compound with a primitive $BaHg_{11}$ type crystal structure and the *Pm*3*m* space group (Pearson symbol tI10/1). The lattice parameter is accepted to be 8.514 Å corresponding to a compound density of 3.45 g/cm^3. The microhardness is about HV 420 and the CTE is $(20-21)\times10^{-6}$ K^{-1} at 200−500 °C

(4) The Al_8CaCu_4 phase was treated as a strict stoichiometric ternary compound with a tetragonal crystal lattice structure of the $Mn_{12}Th$ type (Pearson symbol tI26/1) same as for the well-known Al_8CeCu_4 phase of the ternary Al−Ce−Cu system. The lattice parameters (a=8.84 Å and c=5.17 Å) are also close to those of the Al_8CeCu_4 phase. The microhardness (~HV 505) and density (4.57 g/cm^3) of the Al_8CaCu_4 phase are the highest among the other Ca-containing phases in the system and the CTE is 18×10^{-6} K^{-1} at 200−500 °C.

CRediT authorship contribution statement

T. K. AKOPYAN: Conceptualization, Supervision, Funding acquisition, Data curation, Writing − Original draft, Review & editing; **T. A. SVIRIDOVA:** Data curation, Methodology, Investigation, Software, Visualization; **N. A. BELOV:** Resources, Methodology, Data curation; **N. V. LETYAGIN:** Investigation, Data curation; **A. V. KOROTITSKIY:** Investigation, Data curation.

Declaration of competing interest

The authors declare that they have no known competing financial interests or personal relationships that could have appeared to influence the work reported in this paper.

Data availability

The raw/processed data required to reproduce these findings cannot be shared at this time due to technical or time limitations.

Acknowledgments

The study was carried out with the financial support of Federal Academic Leadership Program, Russia (Priority 2030 of NUST MISIS).

References

[1] BAHL S, PLOTKOWSKI A, SISCO K, LEONARD D N, ALLARD L F, MICHI R A, POPLAWSKY J D, DEHOFF R, SHYAM A. Elevated temperature ductility dip in an additively manufactured Al−Cu−Ce alloy [J]. Acta Materialia, 2021, 220: 117285.

[2] BELOV N A, KHVAN A V, ALABIN A N. Microstructure and phase composition of Al−Ce−Cu alloys in the Al-rich corner [J]. Materials Science Forum, 2006, 519/520/521: 395−400.

[3] POZDNIAKOV A V, BARKOV R Y, AMER S M, LEVCHENKO V S, KOTOV A D, MIKHAYLOVSKAYA A V. Microstructure, mechanical properties and superplasticity of the Al−Cu−Y−Zr alloy [J]. Materials Science and Engineering: A, 2019, 758: 28−35.

[4] LIN Gao-yong, LI Kun, FENG Di, FENG Yong-ping, SONG Wei-yuan, XIAO Meng-qiong. Effects of La−Ce addition on microstructure and mechanical properties of Al−18Si−4Cu−0.5Mg alloy [J]. Transactions of Nonferrous Metals Society of China, 2019, 29: 1592−1600.

[5] LIAO Heng-cheng, XU He-ting, HU Yi-yun. Effect of RE addition on solidification process and high-temperature strength of Al−12%Si−4%Cu−1.6%Mn heat-resistant alloy [J]. Transactions of Nonferrous Metals Society of China, 2019, 29: 1117−1126.

[6] YUNUSOV I, GANIEV I N, SHISHKIN E A. The aluminum rich corner of the Al−Cu−Ce phase diagram [J]. Izvestia Akademii nauk SSSR. Metally, 1991, 3: 200−203.

[7] BELOV N A, KHVAN A V. The ternary Al−Ce−Cu phase diagram in the aluminum-rich corner [J]. Acta Materialia, 2007, 55: 5473−5482.

[8] BO H, JIN S, ZHANG L G, CHEN X M, CHEN H M, LIU L B, ZHENG F, JIN Z P. Thermodynamic assessment of Al−Ce−Cu system [J]. Journal of Alloys and Compounds, 2009, 484: 286−295.

[9] ZHANG L, MASSET P J, TAO X, HUANG G, LUO H, LIU L, JIN Z. Thermodynamic description of the Al−Cu−Y ternary system [J]. Calphad: Computer Coupling of Phase

Diagrams and Thermochemistry, 2011, 35: 574−579.

[10] JIN L, KANG Y B, CHARTRAND P, FUERST C D. Thermodynamic evaluation and optimization of Al−La, Al−Ce, Al−Pr, Al−Nd and Al−Sm systems using the modified quasichemical model for liquids [J]. Calphad: Computer Coupling of Phase Diagrams and Thermochemistry, 2011, 35: 30−41.

[11] YANG Q, LIU X J, BU F Q, MENG F Z, ZHENG T, ZHANG D P, MENG J. First-principles phase stability and elastic properties of Al−La binary system intermetallic compounds [J]. Intermetallics, 2015, 60: 92−97.

[12] TANG C Y, DU Y, XU H H, XIONG W, ZHANG L J, ZHENG F, ZHOU H Y. Experimental investigation of the Al−Ce−Ni system at 800 °C [J]. Intermetallics, 2008, 16: 432−439.

[13] MANCA D R, CHURYUMOV A Y, POZDNIAKOV A V, PROSVIRYAKOV A S, RYABOV D K, KROKHIN A Y, KOROLEV V A, DAUBARAYTE D K. Microstructure and properties of novel heat resistant Al−Ce−Cu alloy for additive manufacturing [J]. Metals and Materials International, 2019, 25: 633−640.

[14] MISHRA R S, THAPLIYAL S. Design approaches for printability−performance synergy in Al alloys for laser-powder bed additive manufacturing [J]. Materials & Design, 2021, 204: 109640.

[15] BAHL S, SISCO K, YANG Y, THESKA F, PRIMIG S, ALLARD L F, MICHI R A, FANCHER C, STUMP B, DEHOFF R, SHYAM A, PLOTKOWSKI A. Al−Cu−Ce(−Zr) alloys with an exceptional combination of additive processability and mechanical properties [J]. Additive Manufacturing, 2021, 48: 102404.

[16] BELOV N A, NAUMOVA E A, AKOPYAN T K, DOROSHENKO V V. Design of multicomponent aluminium alloy containing 2 wt.% Ca and 0.1 wt.% Sc for cast products [J]. Journal of Alloys and Compounds, 2018, 762: 528−536.

[17] BELOV N A, NAUMOVA E A, AKOPYAN T K. Effect of 0.3 wt.% Sc on microstructure, phase composition and hardening of Al−Ca−Si eutectic alloys [J]. Transactions of Nonferrous Metals Society of China, 2017, 27: 741−746.

[18] AKOPYAN T K, BELOV N A, LUKYANCHUK A A, LETYAGIN N V, SVIRIDOVA T A, PETROVA A N, FORTUNA A S, MUSIN A F. Effect of high pressure torsion on the precipitation hardening in Al−Ca−La based eutectic alloy [J]. Materials Science and Engineering: A, 2021, 802: 140633.

[19] AKOPYAN T K, BELOV N A, NAUMOVA E A, LETYAGIN N V, SVIRIDOVA T A. Al-matrix composite based on Al−Ca−Ni−La system additionally reinforced by $L1_2$ type nanoparticles [J]. Transactions of Nonferrous Metals Society of China, 2020, 30: 850−862.

[20] AKOPYAN T K, LETYAGIN N V, SVIRIDOVA T A, KOROTKOVA N O, PROSVIRYAKOV A S. New casting alloys based on the Al+Al_4(Ca,La) eutectic [J]. JOM, 2020, 72: 3779−3786.

[21] BELOV N A, NAUMOVA E A, AKOPYAN T K, DOROSHENKO V V. Phase diagram of the Al−Ca−Fe−Si system and its application for the design of aluminum matrix composites [J]. JOM, 2018, 70: 2710−2715.

[22] LUO G, ZHOU X, LI C B, DU J, HUANG Z H. Design and preparation of Al−Fe−Ce ternary aluminum alloys with high thermal conductivity [J]. Transactions of Nonferrous Metals Society of China, 2022, 32: 1781−1794.

[23] LETYAGIN N V, SHURKIN P K, NGUEN Z, KOSHMIN A N. Effect of thermodeformation treatment on the structure and mechanical properties of the $Al_3Ca_1Cu_{1.5}Mn$ alloy [J]. Physics of Metals and Metallography, 2021, 122: 814−819.

[24] LETYAGIN N V, MUSIN A F, SICHEV L S. New aluminum−calcium casting alloys based on secondary raw materials [J]. Materials Today: Proceedings, 2021, 38: 1551−1555.

[25] KAUFMAN L, AGREN J. CALPHAD, first and second generation – Birth of the materials genome [J]. Scripta Materialia, 2014, 70: 3−6.

[26] HARI KUMAR K C, WOLLANTS P. Some guidelines for thermodynamic optimization of phase diagrams [J]. Journal of Alloys and Compounds, 2001, 320: 189−198.

[27] SCHMID-FETZER R, ANDERSSON D, CHEVALIER P Y, ELENO L, FABRICHNAYA O, KATTNER U R, SUNDMAN B, WANG C, WATSON A, ZABDYR L, ZINKEVICH M. Assessment techniques, database design and software facilities for thermodynamics and diffusion [J]. Calphad, 2007, 31: 38−52.

[28] SHELEKHOV E V, SVIRIDOVA T A. Programs for X-ray analysis of polycrystalline [J]. Metal Science and Heat Treatment, 2000, 42: 309−313.

[29] ANDERSSON J O, HELANDER T, HÖGLUND L, SHI P, SUNDMAN B. Thermo-calc and DICTRA, computational tools for materials science [J]. Calphad, 2002, 26: 273−312.

[30] MONDOLFO L F. Aluminum alloys: Structure and properties [M]. London: Butterworths and Co., Ltd., 1976.

[31] DELAHAYE J, TCHUINDJANG J T, LECOMTE-BECKERS J, RIGO O, HABRAKEN A M, MERTENS A. Influence of Si precipitates on fracture mechanisms of $AlSi_{10}Mg$ parts processed by selective laser melting [J]. Acta Materialia, 2019, 175: 160−170.

[32] ZHU A W, STARKE E A. Strengthening effect of unshearable particles of finite size: A computer experimental study [J]. Acta Materialia, 1999, 47: 3263−3269.

[33] WU T, DUNAND D C. Microstructure and thermomechanical properties of $Al_{11}Ce_3$ [J]. Intermetallics, 2022, 148: 107636.

[34] ZOGG H, SCHWELLINGER P. Phase transformation of the intermetallic compound Al_4Ca [J]. Journal of Materials Science, 1979, 14: 1923−1932.

[35] PREDEL F. Phase equilibria, crystallographic and thermodynamic data of binary alloys: K−O … Y−Zr [M]. Heidelberg: Springer, 2016.

Al−Ca−Cu 三元合金体系中与铝平衡的金属间化合物

T. K. AKOPYAN, T. A. SVIRIDOVA, N. A. BELOV, N. V. LETYAGIN, A. V. KOROTITSKIY

National University of Science and Technology MISiS, 4 Leninsky pr., Moscow 119049, Russia

摘　要：对三元 Al−Ca−Cu 合金体系中与铝固溶体平衡的 $(Al,Cu)_4Ca$、$Al_{27}Ca_3Cu_7$ 和 Al_8CaCu_4 金属间化合物的结构和性能进行全面分析。基于 Al_4Ca 相中部分 Al 原子被 Cu 取代，将$(Al,Cu)_4Ca$ 金属间化合物视为线性化合物。化合物中铜的溶解度达到 10 at.%(19 wt.%)，导致化合物的晶格结构、物理和力学性能发生显著变化。例如，化合物的密度从 2.22 g/cm^3 增加到 2.79 g/cm^3，显微硬度从 HV 180 增加到 HV 250。将 $Al_{27}Ca_3Cu_7$ 相视为具有严格化学计量比和 $BaHg_{11}$ 型初始晶体结构的三元化合物，其空间群为 $Pm3m$，晶格参数为 8.514 Å，密度为 3.45 g/cm^3。Al_8CaCu_4 相也是严格化学计量比的三元化合物，具有 $Mn_{12}Th$ 型晶格结构，最高的显微硬度(HV 505)和密度(4.57 g/cm^3)。属于二元(Al) + $(Al,Cu)_4Ca$ 相场和准二元(Al) + $Al_{27}Ca_3Cu_7$ 截面的合金，有前景作为新型天然铝基复合材料的基材。

关键词：金属间化合物；Al−Ca 合金；显微组织；晶体结构；物理性能；力学性能

(Edited by Wei-ping CHEN)